ZIBELINE INTERNATIONAL™ PUBLISHING

Engineering Heritage Journal (GWK)

DOI: http://doi.org/10.26480/gwk.02.2025.60.65

ISSN: 2521-0904 (Print)
ISSN: 2521-0440 (Online)
CODEN: EHJNA9

RESEARCH ARTICLE

ENHANCING CERAMIC PROPERTIES WITH TUNISIAN KEF ABED CLAY AND SEDIMENTARY ROCK BLENDS

Mohamed Benmohamed[a], Marouene Bejaoui[a]*, Imen Khedhri[a], Ayechi Mohamed Slim[a], Noureddine Ben Aoun[a], RabahAlouani[b], Benhaj Amara Abdesslem[a]

[a] LR Ressource Matériaux et Ecosystème, Matériaux Lamellaire et Nanomatériaux Hybrides, Faculté des Sciences de Bizerte, Université de Carthage, 7021 Bizerte, Tunisia
[b] Département des sciences de la terre, faculté des sciences de Bizerte, Université de Carthage
****Corresponding author email: marouene2010@gmail.com***

ARTICLE DETAILS

Article History:

Received 17 September 2025
Revised 20 October 2025
Accepted 24 November 2025
Available online 30 December 2025

ABSTRACT

This study explores the potential use of Tunisian raw materials in ceramic applications. Clay mineral collected from Kef Abed (KA) in northern Tunisia (Numidian zone) was blended with limestone (Abiod formation) and dolomitic sedimentary rock as auxiliary fluxes in ceramic bodies. The Kef Abed clay is predominantly kaolinitic, with other associated minerals such as illite, smectite, quartz, feldspar, and hematite. Two different granulometry distributions of KA clay were blended with varying percentages of limestone (5%, 15%, and 25%), while dolomite was used at a fixed percentage (5%). Ceramic bodies were formed by pressing at 7 tons and subsequently fired at 500°C, 750°C, and 1000°C. The chemical and mineralogical compositions were analyzed using ICP and X-ray diffraction, respectively. FTIR and TG-DTA were employed to characterize the raw and purified KA clay samples, while TEM images were used to investigate the fired materials. The thermal behavior study of KA clay (both raw and purified) using X-ray data and TEM images revealed the presence of a mullite phase, with its quantity increasing as the granulometry decreased. Mineralogical analysis indicated that ceramics tempered with 5% limestone and 5% dolomite are particularly suitable for ceramic applications.

KEYWORDS

ceramics, thermal behaviour, granulometry, clay mineral, mullite

1. INTRODUCTION

From a process control Clay rocks have long been fundamental to ceramic production, being used to manufacture both low- and high-porosity ceramic materials (Maniatis and Tite, 1981). To improve the workability and technological performance of natural clays, numerous studies have investigated their modification through tempering with various materials (Rice, 1987; Tite, 2008; Rye, 1976; Cultrone and Rosua, 2020). These tempers include natural raw materials such as quartz and limestone, as well as recycled waste materials, including gneiss rock waste, waste clay, and granite sawing residues (Allegretta et al., 2014; Cristina et al., 2020; Souza et al., 2010; Menezes et al., 2005; Jain et al., 2020).

Mullite is highly valued in ceramic materials owing to its outstanding properties, such as low thermal expansion, excellent creep resistance, high chemical and thermal stability, superior mechanical strength at elevated temperatures, low thermal conductivity, low density, a very low dielectric constant, and good optical characteristics (Chen et al., 2003; Roy et al., 2022).

The formation of mullite is governed by several factors, including the particle size and crystalline nature of the precursors, the Al/Si ratio, the degree of homogeneity achieved during mixing, and the presence of impurities (Okada and Otsuka, 1991). Structurally, mullite is closely related to sillimanite (Schneider et al., 2008). Nevertheless, species diffusion plays a crucial role in the mullite phase transformation, strongly influencing nucleation and grain growth. The crystallization kinetics of mullite generally proceeds through multiple stages, namely nucleation, nucleation–growth, and coalescence (Takei et al., 1999; Hildmann, et al., 1996; Li and Thomson, 1990; Rye, 1976; Cultrone and Rosua, 2020).

Global demand for clay has increased markedly in recent years, particularly in Tunisia, where technological advances have broadened its applications to ceramics, pharmaceuticals, and environmental protection, such as clay barriers in landfill systems. Consequently, numerous studies have focused on Tunisian clays and their potential applications (Khemakhem et al., 2009; Baccour et al., 2008; Felhi et al., 2008; Baccour et al., 2009; Hajjaji et al., 2010; Moussi et al., 2011; Bennour, et al., 2015; Mahmoudi, et al., 2016; Moussi, et al., 2020; Bousbih et al., 2021). Over the past decades, several investigations have examined Tunisian clays as raw materials for ceramic products, with particular attention to those originating from the Flysch Formation (Bennour, et al., 2015; Moussi, et al., 2020; Chalouati, et al., 2020; Mahmoudi and Bennour, 2022). Among these, Numidian clays from the Flysch Formation have been extensively studied for their suitability in ceramic applications (Bennour, et al., 2015; Moussi, et al., 2020).

Kef Abed clay, belonging to the Numidian zone, was collected from the Kef Abed quarry in northern Tunisia. This clay is rich in kaolinite and contains several associated mineral phases. In the present study, Tunisian natural raw materials—namely limestone, dolomitic rock, and Kef Abed clay—were investigated for their potential use in ceramic applications (Rouvier, 1977). Limestone was incorporated into the clay fraction at levels of 5%, 15%, and 25%, while dolomitic rock was added as an auxiliary flux at a fixed proportion of 5%. In addition, different clay particle-size fractions were evaluated.

Quick Response Code	Access this article online	
	Website: www.gwk.com.my	**DOI:** 10.26480/gwk.02.2025.60.65

Cite The Article: Mohamed Benmohamed, Marouene Bejaoui, Imen Khedhri, Ayechi Mohamed Slim, Noureddine Ben Aoun, RabahAlouani, Benhaj Amara Abdesslem (2025). Enhancing Ceramic Properties With Tunisian Kef Abed Clay And Sedimentary Rock Blends. *Engineering Heritage Journal (GWK)*, 9(2): 60-65

2. Geological Setting

The study area is situated at an altitude of approximately 248 meters within the Séjnen region, with geographical coordinates of 37°15'24" N and 9°26'3" E (UTM position: NG32). It is located in the middle limb of the Numidian flysch, corresponding to the Kroumirie sandstone series (Madejova, 2003; Njoya et al., 2006; Djangang et al., 2007; Nkoumbou, et al., 2006). The site, Kef Abed, dates back to the Upper Oligocene and Miocene periods (Oligo-Miocene), and is characterized by sandstones, conglomerates, and clays, forming a layer approximately 130 meters thick (Figure 1).

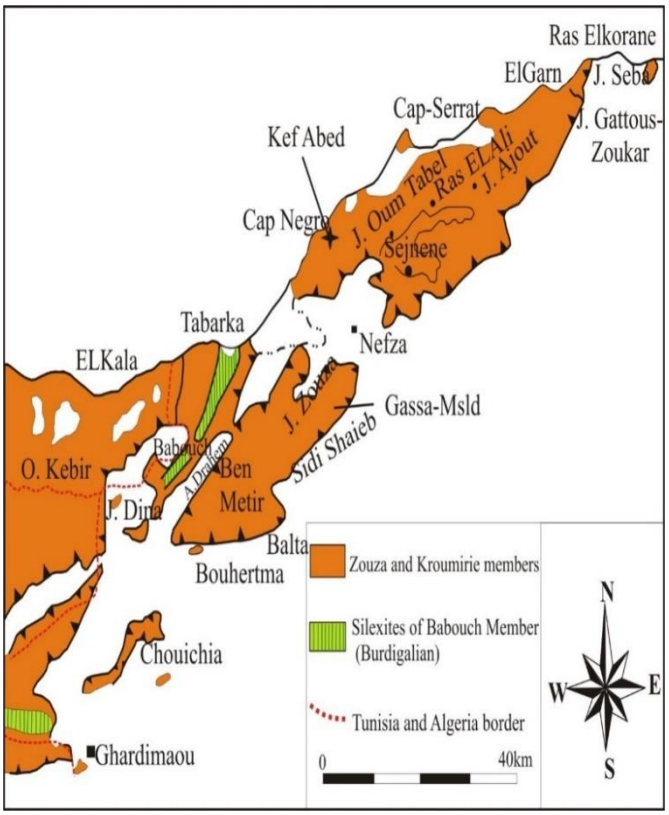

Figure 1: Numidian flysh in north Tunisia and the geological situation of the studied clays deposits samples [30].

3. Experimental Details

KA clay was prepared to determine its thermal behavior. The clay fraction was separated using the centrifugation method. The KA powder, both purified (P) and raw (B), was pressed under 7 tonnes of pressure to form discs with a diameter of 3 cm and a thickness of 3.5 mm. The samples were dried for 24 hours at 100 °C and subsequently heated to assess mineralogical transformations at temperatures of 300, 600, 800, 1000, and 1200 °C for three hours. To prepare ceramic bodies, two fractions (63 and 106 µm) of ground KA powder were selected (Brown and Brindley, 1984). The ground agglomerates were mixed with 5%, 15%, and 25% of limestone (Abiod formation) as a temper, and 5% dolomitic rock was added as an auxiliary flux (Table 1). The raw mix was homogenized and humidified to 6 wt. % water content. The mixture was then pressed under 7 tonnes of pressure to form discs with a diameter of 30 mm and a thickness of 3.5 mm (Carty and Senapati, 1998). The discs were dried at 100 °C for 24 hours and subsequently fired at 500, 750, and 1000 °C with a heating rate of 150 °C/h and a soaking time of 1 hour. The firing temperatures were chosen to simulate the actual firing process used in the ceramics industry (Jung et al., 2001).

Table 1: The mixture prepared with raw materials composition (in weight % and g); the mixtures M1, M2, and M3 were prepared using two granulometry (63µm and 106µm)

Mixture	M1	M2	M3
Raw material (Weight (%))	5% dolomite 5% limestone 90% clay (KA)	5% dolomite 15% limestone 80 % clay (KA)	5% dolomite 25% limestone 70 clay (KA)
Raw material (Weight (g))	0.3g dolomite 0.3g limestone 5.4g clay (KA)	0.3g dolomite 0.9 limestone 4.8 clay (KA)	0.3g dolomite 1.5g limestone 4.2g clay (KA)
Mixture	**M1**	**M2**	**M3**
Raw material (Weight (%))	5% dolomite 5% limestone 90% clay (KA)	5% dolomite 15% limestone 80 % clay (KA)	5% dolomite 25% limestone 70 clay (KA)
Raw material (Weight (g))	0.3g dolomite 0.3g limestone 5.4g clay (KA)	0.3g dolomite 0.9 limestone 4.8 clay (KA)	0.3g dolomite 1.5g limestone 4.2g clay (KA)

4. Characterization Of The Materials

The mineralogical composition was determined using X-ray diffraction (D8 Advance diffractometer). X-ray data were collected at room temperature using Bragg-Brentano geometry (θ, 2θ) with Cu-Kα radiation (λ = 1.5406 Å). The X-ray tube was operated at 40 kV and 40 mA. To obtain the clay fraction (<2 µm), the raw material was purified using sedimentation techniques (Zhang et al., 2014; Aydin et al., 2019; Lee, et al., 1999; Chakraborty, 2003). Organic matter was removed by adding a small amount of H2O2, followed by decarbonation with 1M HCl. The clay fraction was then separated using centrifugation and suspension methods. Semi-quantitative analysis was conducted on oriented aggregates treated with ethylene glycol and heated to 550 °C for 2 hours. XRD patterns were recorded from 3.5° to 60° for raw material powder, while oriented aggregates were recorded from 3.5° to 40°. Chemical analysis was carried out using inductively coupled plasma mass spectrometry (ICP-MS) to determine the chemical composition of the raw materials. The morphology of the fired clay samples was analyzed using transmission electron microscopy (TEM).

5. Results And Discussion

Table 2 presents the chemical composition (by weight %) of the raw materials used in this study:

5.1 KA Clay

The chemical composition of natural (P) and purified (B) KA clay samples is presented in Table 2. Both samples are predominantly composed of SiO_2 and Al_2O_3, with concentrations of 55.37% and 57.29%, respectively. Minor constituents include Fe_2O_3 (4.5% and 1.5%), K_2O (2.5% and 2.8%), and MgO (1.5% and 1.3%). The elevated K_2O content in the purified sample is indicative of the presence of illite. The low Fe_2O_3 content suggests only a limited amount of hematite, while the detected MgO points to the presence of smectite. Additional minor components, such as CaO and SO_3, are also detected, though in negligible amounts.

5.2 Limestone (Abiod Formation)

The limestone is characterized by low hardness, a high CaO content (>54%), and minimal amounts of coloring metal oxides, primarily Fe2O3 and Ti2O3. This composition results in a high degree of whiteness ($\beta \approx 85.34$).

5.3 Dolomitic Rock

This rock is whitish with low hardness and high CaO content (26.67%), followed by SiO2 (16.59%) and MgO (24.11%). The small amount of Al2O3 (2.53%) is due to the presence of a minor quantity of kaolinite, along with other insignificant oxides such as Fe2O3 (1.82%) and SO3 (1.06%).

Table 2: Chemical composition of raw materials in percentages oxides (weight %)

Element (%)	SiO_2	Al_2O_3	Fe_2O_3	CaO	K_2O	MgO	SO_3	TiO_2	LOI
KA (B)	55.37	18.5	4.5	0.15	2.5	1.5	0.3	0.18	15
KA (P)	57.29	21.5	1.5	0.11	2.8	1.3	-	-	15.5
Limestone	0,80	0,34	0,11	54,5	0.00	0,04	--	0,02	43,42
Dolomitic rocks	16.59	2.53	1.82	26.67	0.05	24.11	1.06	0.00	24

The X-ray powder diffraction data for bulk KA clay (Figure 2) reveal a significant percentage of phyllosilicates, including kaolinite (>70%), smectite (~20%), and illite (>6%), along with quartz, feldspar, and hematite. Oriented aggregate analysis shows that the clay fraction (<40

µm) is predominantly composed of kaolinite. Quartz is the main mineral in the rock, followed by feldspar and hematite. Figure 3 presents the X-ray powder diffraction patterns for limestone and dolomite used in the ceramic mixture. Limestone is primarily composed of calcite, while dolomite shows minor impurities such as quartz and phyllosilicate.

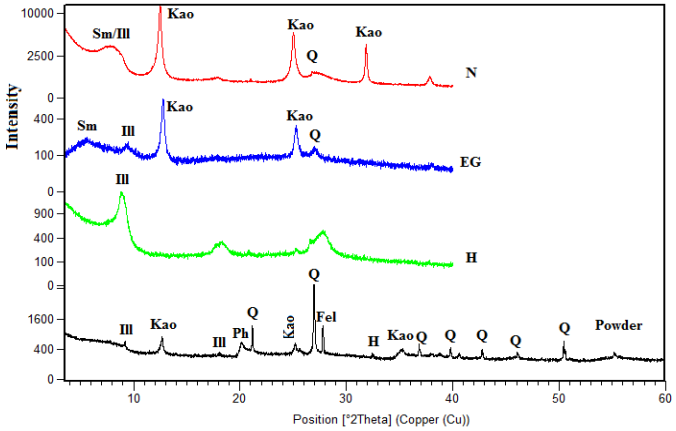

Figure 2: X-ray patterns of the bulk sample (powder) and oriented aggregate (<40µm); N: unprocessed sample, EG: treated with ethylene glycol, H: heated at 550 °C. Ill: illite, Kao: Kaolinite, Sm: Smectite, Ph: Phyllosilicate, Q: Quartz, Fel: Feldspar, H: Hematite.

The OH-stretching region of kaolinite exhibits two bands at 3694 and 3669 cm^{-1}. The band at 3694 cm^{-1} corresponds to the in-phase coupled stretching vibration of perpendicular surface OH groups, whereas the band at 3669 cm^{-1} arises from the out-of-phase coupling of kaolinite. Illite, kaolinite, and smectite show a prominent band at 3622 cm^{-1} due to hydroxyl group vibrations, along with additional absorption around 3410 cm^{-1}. In the Si–O stretching region, a band at 1033 cm^{-1} is assigned to octahedral smectite, while the band at 915 cm^{-1} corresponds to illite. The purified sample displays a similar IR pattern (Figure 4), with minor shifts reflecting the reduced impurity content.

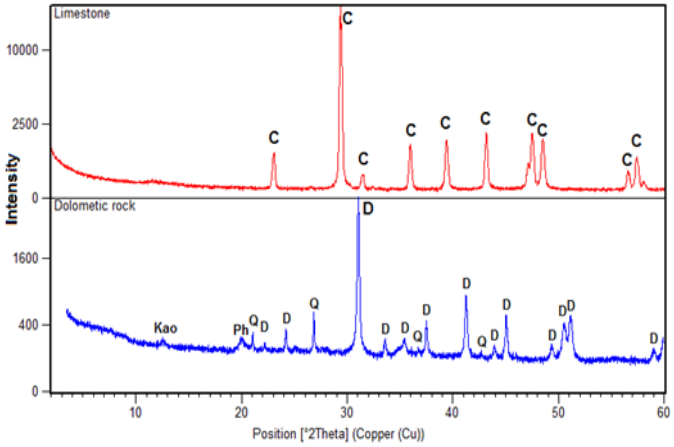

Figure 3: X-ray patterns of raw materials (limestone and dolomite rock); Calcite(C), dolomite(D),quartz(Q), kaolinite (Kao), Phyllosilicate (Ph).

The DTA-TG analysis of the KA sample (Figure 5P) reveals three endothermic peaks in the DTA curve. Two inflections between 50 and 95 °C are attributed to the loss of physically adsorbed water. The curve also displays an endothermic peak at 515 °C and an exothermic peak at 992 °C, characteristic of kaolinite minerals. The main endothermic peak, observed between 400 and 600 °C, corresponds to kaolinite dehydration. A high-intensity peak suggests the presence of a small amount of impurities in KA (P). This endothermic inflection is accompanied by weight loss in the DTG curve (Δm (%) = -7.752), associated with the dehydroxylation of sheet silicates, indicating a negligible quantity of other minerals. A minor weight loss between 200 and 350 °C likely reflects the dehydration of illite, which initiates around 200 °C.

The DTA-TG profile of the purified KA sample (Figure 5B) is generally similar, although the kaolinite peaks are weaker, indicating a higher impurity content. Additionally, a small endothermic peak between 606 and 620 °C suggests quartz inversion (α- to β-quartz). Between 875 and 1025 °C, small exothermic peaks are observed, attributed to mullite nucleation or the dissociation of metakaolinite.

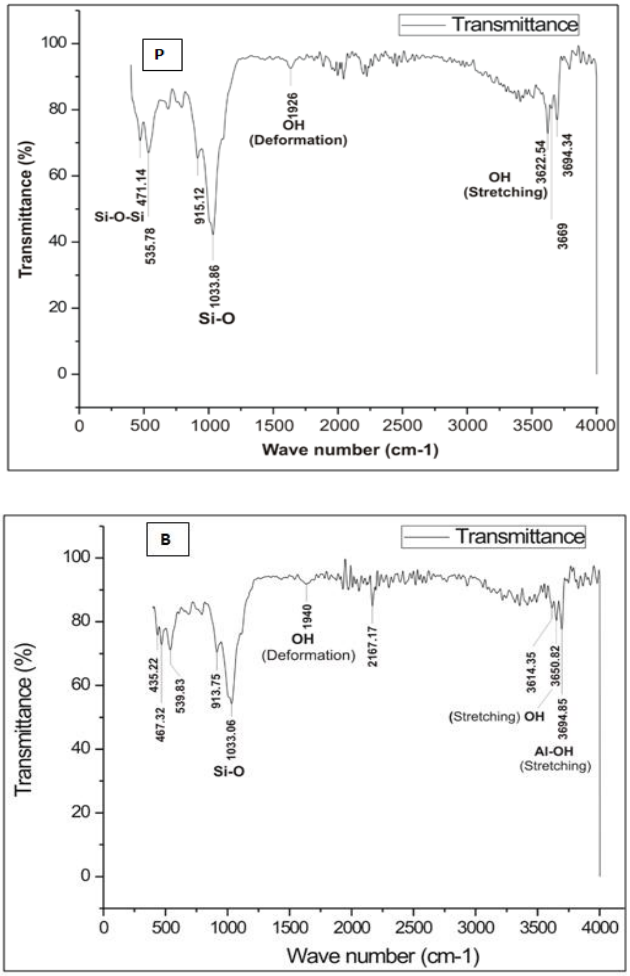

Figure 4: IR spectra of clay KA (P and B) wave number ranging between 400–4000 cm^{-1}

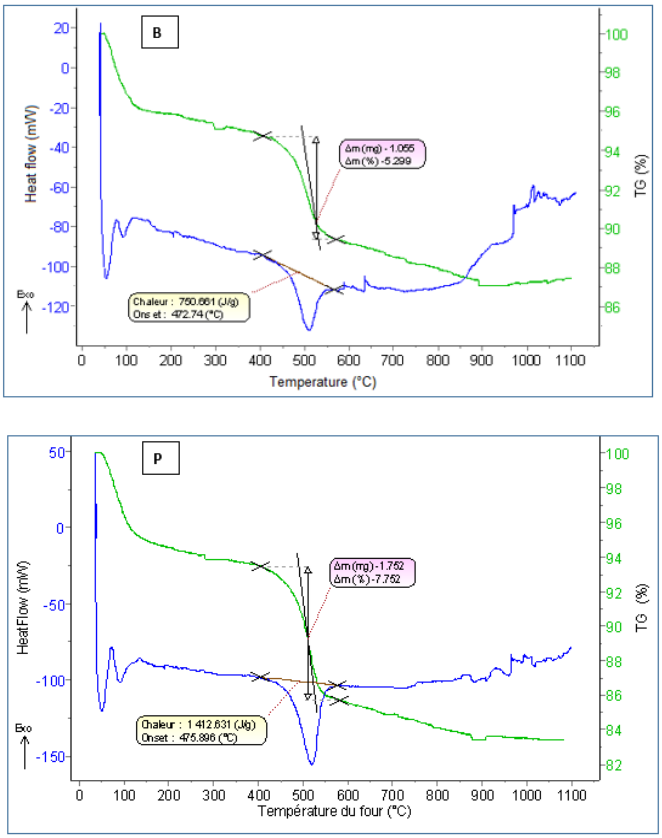

Figure 5: Thermal analysis curves DTA/TG diagrams of KA clay 5B (brute) and 5P (pure)

As shown in Figure 6, the X-ray patterns of purified KA (P) fired at temperatures between 300 and 1200 °C exhibit significant variations in mineralogical phases. At 300 °C, sheet minerals (kaolinite, illite, and smectite) are present with a small amount of quartz. At 600 °C, kaolinite is completely transformed into metakaolinite according to the reaction: ($2Al_2Si_2O_5(OH)_4 \rightarrow 2Al_2Si_2O_7 + 4H_2O$) which begins at 550 °C as noted in the literature. This transformation is accompanied by an increase in free quartz. At 1000 °C, phyllosilicate minerals disappear completely, and the maximum amount of free quartz and large humps indicating the amorphous phase are observed. Mullite first appears at 1000 °C, with the neoformed phases becoming more pronounced at 1200 °C. At this temperature, mullite, sillimanite, cristobalite, and hexagonal quartz begin to form. The KA clay (B) heated from 300 to 1200 °C shows quartz as the major phase, with minor amounts of feldspar (Figure 7).

A small quantity of mullite appears at 1000 °C. The results obtained from sintering the clay fraction and the raw clay indicate that the formation of ceramic phases is related to the chemical composition and granulometry of the clay. The shape and size of mullite particles influence key properties of the fired material, including pore structure and fracture strength. The mineralogical composition of pure sintered clay at 1200 °C was determined using X-ray powder diffraction, and the profiles are displayed in Figure 8. Quantitative analysis based on the results in Figure 8 shows the presence of two major phases: Sillimanite (65.3%) and Mullite (21.6%). Minor phases include Quartz (hexagonal, 8.5%) and Cristobalite (4.7%). Rietveld refinement was performed using the X'Pert HighScore program (PANalytical version, 2013), yielding a low agreement index (Rwp = 8.45 and Gof = 1.22).

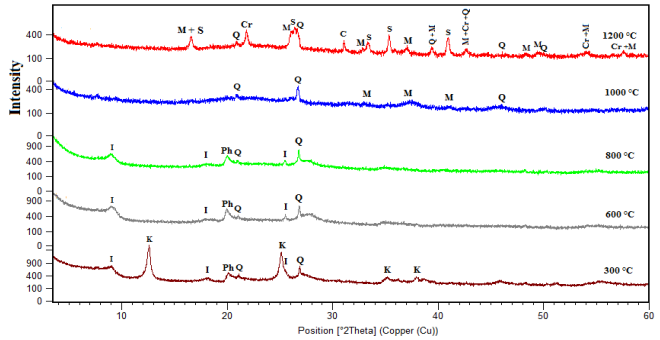

Figure 6: X-ray powder diffraction patterns of purified KA clay (P) fired at temperatures 300 °C, 600 °C, 800 °C, 1000 °C, and 1200 °C; Kaolinite (K), Illite (I),Phyllosilicate (Ph),Quartz(Q), Mullite(M),Cristobalite(Cr)

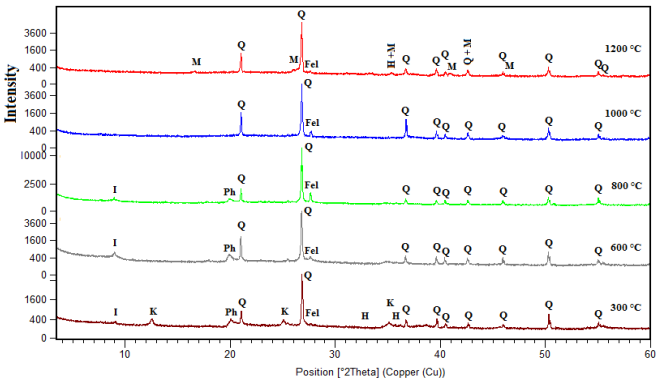

Figure 7: X-ray powder diffraction patterns of brute KA clay (B) fired at temperatures 300 °C, 600 °C, 800 °C, 1000 °C, 1200 °C. Kaolinite(K), Illite(I), Ph, Phyllosilicate, Quartz(Q),Mullite(M)

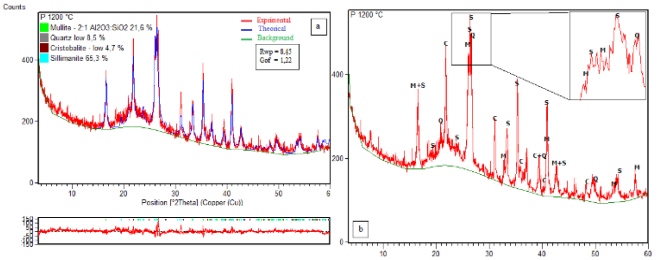

Figure 8: X-ray powder diffraction pattern of clay (P) (sample sintered at 1200 °C); a: the quantitative analysis, b: the identification of phases (M: Mullite, Q: Quartz, S: Sillimanite, Cr: Cristobalite

The morphology of mullite microstructures has been widely investigated in the literature. TEM analysis of KA clay heated to 1200 °C reveals the formation of the mullite phase, with a clear difference in abundance between the purified and raw heated samples (Figure 9). Previous studies report mullite as plate-like crystals, exhibiting a broad size distribution ranging from 20 to 200 nm in length and up to 50 nm in width. At higher magnification (Figure 10), broad crystals of quartz and silica gel are also observed. All newly formed phases are embedded within and stabilized by an amorphous matrix.

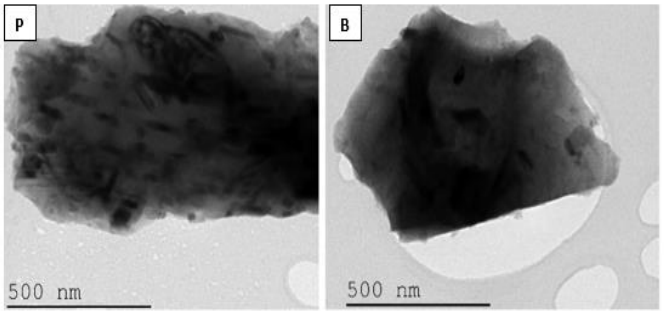

Figure 9: TEM micrographs of clay KA heated at 1200° C; KA (P), KA (B)

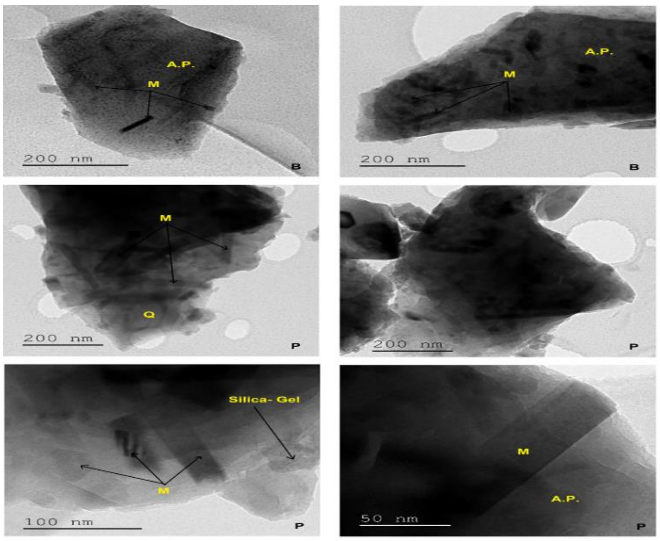

Figure 10: Morphology of mullite shown as plate like forms; Mullite (M), amorphous phase (A.P.)

Figure 11 shows discs fired at 550 °C, 750 °C, and 1000 °C. KA clay was used in two particle size fractions (63 µm and 106 µm) and blended with limestone at varying concentrations (5%, 15%, and 25%), with 5% dolomite added as an auxiliary flux. The resulting materials were subsequently subjected to mineralogical characterization.

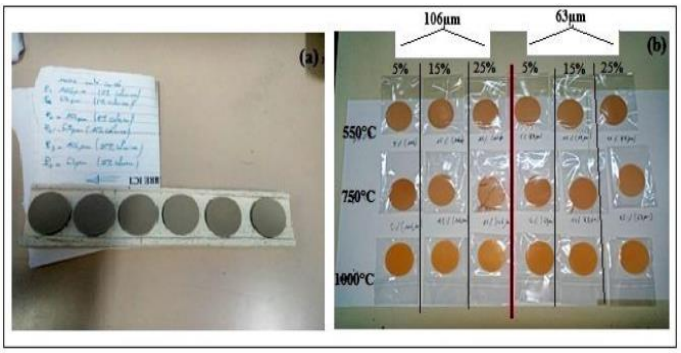

Figure 11: Ceramic bodies prepared as disks fired at different temperatures (550, 750, and 1000 °C) and concentrations of limestone (5, 15, 25%)

The curves in Figure 12 illustrate the variation in weight loss of ceramic bodies with increasing temperature and granulometry. While particle size showed no significant variation, an increase in limestone concentration led to greater weight loss due to the calcination of limestone.

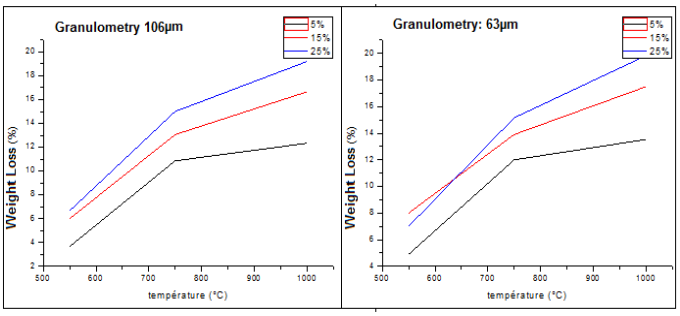

Figure 12: Weight loss in function of temperature and temper concentration

The chemical composition of the raw materials and the firing temperature of the mixture strongly influence the color of the ceramic body, which ranges from yellow to red. Samples tempered with 15% and 25% limestone and fired at 750 °C and 1000 °C showed deterioration due to lime spalling. The main neoformed phases in samples fired at these temperatures include portlandite, formed by lime hydration, and gehlenite, which appears only in samples containing 25% limestone. An amorphous phase is present in all samples, as indicated by the small hump in the XRD pattern, accompanied by a spinel-like phase and traces of poorly crystallized mullite. Literature reports indicate that the amorphous phase accounts for 18–40 wt%, the spinel phase 25–35 wt%, and mullite 4–8 wt%. The spinel-like phase has been identified as α-Al_2O_3, characterized by low silica content.

6. Conclusion

Kef Abed (KA) clays, derived from the Oligo-Miocene Numidian flysch in northern Tunisia, are characterized by relatively high kaolinite content and low iron levels. This study focused on basal samples composed of kaolinite, smectite, and illite, with minimal iron impurities. Thermal analysis of both raw and purified clays underscores the crucial role of granulometry in controlling the formation of key ceramic minerals, such as mullite and sillimanite, whose abundance depends on chemical composition and particle size. These clays, rich in fluxing elements, exhibit favorable chemical and mineralogical properties at 550 °C, producing a yellowish to reddish coloration. When KA clay was tempered with limestone (Abiod) at low concentrations (5%) and dolomite as an auxiliary flux (5%), the resulting ceramic products displayed satisfactory quality. However, higher limestone additions (15% and 25%) led to deterioration due to lime spalling, causing portlandite formation one month after sintering.

References

Allegretta, I., Eramo, G., Pinto, D., Hein, A., 2014. The effect of temper on the thermal conductivity of traditional ceramics: nature, percentage and granulometry. Thermochim. Acta, 581, 100-109, https://doi.org/10.1016/j.tca.2014.02.024.

Aydin, T., Bican, O., Gümrük, R., 2019. Investigation of wear resistance of the porcelain tile bodies by solid particle impingement using alumina particles. Journal of the Australian Ceramic Society, https://doi.org/10.1007/s41779-019-00362-2.

Baccour, H., Medhioub, M., Jamoussi, F., Mhiri, T., Daoud, A., 2008. Mineralogical Evaluation and Industrial Applications of the Triassic Clay Deposits, Southern Tunisia. Materials Characterization, 59, 1613-1622, http://dx.doi.org/10.1016/j.matchar.2008.02.008.

Baccour, H., Medhioub, M., Jamoussi, F., Mhiri, T., 2009. Influence of firing temperature on the ceramic properties of Triassic clays from Tunisia. Journal of Materials Processing Technology, 209 (6), 2812–2817.

compacting concrete by using granite waste and fly ash. Construction and Building Materials, 262 (30) 120-516,https://doi.org/10.1016/j.conbuildmat.2020.120516.

Jung, J.S., Park, H. C., Stevens, S., 2001. Mullite ceramics derived from coal fly ash. J. Mater. Sci. Lett., 20, 1089–1091. https://doi.org/10.1023/A:1010934728570.

Khemakhem, S., Larbot, A., Ben Amar, R., 2009. New ceramic microfiltration membranes from Tunisian natural materials: Application for the cuttlefish effluents treatment. Ceramics International, 35(1), 55–61. https://doi.org/10.1016/j.ceramint.2007.09.117.

https://doi.org/10.1016/j.jmatprotec.2008.06.055.

Bennour, A., Mahmoudi, S., Srasra, E., Boussen, S., Htira, N., 2015. Composition, firing behavior and ceramic properties of the Sejnène clays (Northwest Tunisia). Applied Clay Science, 115, 30–38, https://doi.org/10.1016/j.clay.2015.07.025.

Bousbih, S., Ammar, R.B., Ben Amar, R., Dammak, L., Darragi, F., Selmane, E., 2021. Synthesis and Evaluation of Asymmetric Mesoporous PTFE/Clay Composite Membranes for Textile Wastewater Treatment. Membranes, (11), 850,https://doi.org/10.3390/membranes11110850.

Brown, G., Brindley, G.W., 1984. Crystal Structures of Clay Minerals and their X-ray Identification, Mineral Soc., London 495,https://doi.org/10.1180/mono-5.

Carty, W.M., Senapati, U., 1998. Porcelain-raw materials, processing, phase evolution and mechanical behavior, Am. Ceram. Soc., 8: (1) 3–20. https://doi.org/10.1111/j.1151-2916.1998.tb02290.x.

Chakraborty, A.K., 2003. DTA study of preheated kaolinite in the mullite formation region, Thermochim. Acta, 398, Pp. 203–209,https://doi.org/10.1016/S0040-6031(02)00367-2.

Chalouati, Y., Bennour, A., Mannai, F., Srasra, E., 2020. Characterization, thermal behaviour and firing properties of clay materials from Cap Bon Basin, north-east Tunisia, for ceramic applications. https://doi.org/10.1180/clm.2021.4.

Chen, Y. F., Wang, M. C., Hon, M. H., 2003. Transformation kinetics for mullite in kaolin–Al2O3 ceramics, Journal of Materials Research, 18, (6), Pp. 1355 – 1362. https://doi.org/10.1557/JMR.2003.0186.

Cristina, M. B., Chiara, A., Antonino, P., Marco, V., 2020. An end of waste alternative for volcanic ash: A resource in the manufacture of ceramic tiles. Construction and Buildin Materials, 263 (10) 120-118,https://doi.org/10.1016/j.conbuildmat.2020.120118.

Cultrone, G., Rosua, F. J. C., 2020. Growth of metastable phases during brick firing: Mineralogical and microtextural changes induced by the composition of the raw material and the presence of additives. Applied Clay Science, 185 105-419,https://doi.org/10.1016/j.clay.2019.105419.

Djangang, C. N., Elimbi, A., Nkoumbou, C., Melo, U. C., Yvon, J., Bonnet, J. P., Njopwouo, D., 2007. Characteristics and ceramics properties (1200–1500 C) of clays from Mayouom deposit, West Cameroon, Ind. Ceram., 27, Pp. 79–88,https://doi.org/10.1016/j.ceramint.2007.02.012.

Felhi, M., Tlili, A., Gaied, M. E., Montacer, M., 2008. Mineralogical study of kaolinitic clays from Sidi El Bader in the far north of Tunisia. Applied Clay Science, 39, Pp. 208–451 217,https://doi.org/10.1016/j.clay.2007.06.004.

Hajjaji, W., Moussi, B., Hachani, M., Medhioub, M., Lopez-Galindo, A., Rocha, F., Jamoussi, F., 2010. The potential use of Tithonian–Barremian detrital deposits from central Tunisia as raw materials for ceramic tiles and pigments. Applied Clay Science, 48(4), 552–560,https://doi.org/10.1016/j.clay.2010.03.003.

Hildmann, B. O., Schneider, H., and Schmu¨cker, M., 1996. High temperature behaviour of polycrystalline aluminosilicatefibres with mullite bulk composition. II. Kinetics of mullite formation, J. Eur. Ceram. Soc., 16 (2) 287-292. https://doi.org/10.1016/0955 2219(95)00153-0.

Jain, A., Gupta, R., Chaudhary, S., 2020. Sustainable development of self-

Lee, S., Kim, Y. J., Moon, H. S., 1999. Phase transformation sequence from kaolinite tomullite investigated by an energy-filtering transmission electron microscope, J. Am. Ceram. Soc., 82: 2841–2848, https://doi.org/10.1111/j.1151-2916.1999.tb02165.x.

Li, D. X., Thomson, W. J., 1990. Mullite Formation Kinetics of a Single-Phase Gel, J. Am. Ceram. Soc., 73 (4) 964, https://doi.org/10.1111/j.1151-2916.1990.tb05144.x.

Madejova,J., 2003. FTIR techniques in clay mineral studies,Vibrational Spectroscopy31 (1) 1-10, https://doi.org/10.1016/S0924-2031(02)00065-6.

Mahmoudi, S., Bennour, A., Srasra, E., Zargouni, F., 2016. Determination and adjustment of drying parameters of Tunisian ceramic bodies, Journal of African Earth Sciences. https://doi.org/10.1016/j.jafrearsci.2016.09.031.

Mahmoudi, S., Bennour, A., 2022. Characterisation and ceramic application of clays from North Africa. Applied Earth Science, 131 (1) 15-26, https://doi.org/10.1080/25726838.2021.1992815.

Maniatis, Y., Tite M. S., 1981. Technological examination of Neolithic-Bronze Age pot-tery from Central and Southeast Europe and from the Near East. J. Archaeol. Sci. (8) 59–76. https://doi.org/10.1016/0305-4403(81)90012-1.

Menezes, R. R., Ferreira, H. S., Neves, G. A., Ferreira, H. C., 2005. Use of granite sawing waste in the production of ceramic bricks and tiles. J. Eur. Ceram. Soc., 25 (7), 1149–1158. https://doi.org/10.1016/j.jeurceramsoc.2004.04.020.

Moussi, B., Hajjaji, W., Hachani, M., Hatira, N., Labrincha, J. A., Yans, J., Jamoussi, F., 2020. Numidian clay deposits as raw material for ceramics tile manufacturing. Journal of AfricanEarth Sciences. https://doi.org/10.1016/j.jafrearsci.2020.103775.

Moussi, B., Medhioub, M., Hatira, N., Yans, J., Hajjaji, W., Rocha, F., Labrincha, J. A., Jamoussi, F., 2011. Identification and use of white clayey deposits from the area of Tamra (Northern Tunisia) as ceramic raw materials. Clay Minerals, 46, 165–175,https://doi.org/10.1180/claymin.2011.046.1.165.

Njoya, A., Nkombou, C., Grobois, C., Njopwouo, D., Njoya, D., Courtin-Nomade, A., Yvon, J., Martin, F., 2006. Genesis of Mayouom kaolin (Western Cameroon), Appl. Clay Sci., 32, 125–140. https://doi.org/10.1016/j.clay.2005.11.005.

Nkoumbou, C., Njopwouo, D., Villieras, F., Njoya, A., YontaNgoune, C., Ngo Ndjock, L., Tchoua F., Yvon, J., 2006. Talc indices from Boumnyebel (Central Cameroon), physico-chemical characteristics and geochemistry. J. Afr. Earth Sci. 45 61–73, https://doi.org/10.1016/j.jafrearsci.2006.01.007.

Rice, P.M., 1987. Pottery Analysis: A Sourcebook, first ed., The University of Chicago Press, Chicago.

Rouvier, H., 1977. Géologie de l'Extrême Nord Tunisien: tectoniques et paléogéographies superposées à l'extrémité orientale de la chaîne nord maghrébine. Thèse es Sci. Uni. P. & M. Curie. Paris VI, 703 (Unpublished).

Roy, R., Das, D., Rout, P. K., 2022. A Review of Advanced Mullite Ceramics, Engineerd Science. https://dx.doi.org/10.30919/es8d582.

Rye, O. S., 1976. Keeping your temper under control: materials and the manufacture of Papuan pottery. Archaeol. Phys. Anthropol. Oceania 11, 106–137. https://doi.org/10.1002/j.1834-4453.1976.tb00245.x.

Schneider, H., Schreuer, J., Hildmann, B., 2008. Structure and proprieties of mullite – a review, Journal of the European Ceramic Society, 28 (2), 329-344. https://doi.org/10.1016/j.jeurceramsoc.2007.03.017.

Souza, A. J., Pinheiro, B. C. A., Holanda, J. N. F. 2010. Recycling of gneiss rock waste in the manufacture of vitrified floor tiles. Journal of Environmental Management, 91, 685–689. https://doi.org/10.1016/j.jenvman.2009.09.032.

Takei, T., Kamesshima, Y., Yasumori, A., Okada, K., 1999. Crystallization kinetics of mullite in alumina-silica glass fibers, J. Am. Ceram. Soc., 82, 2876. https://doi.org/10.1111/j.1151-2916.1999.tb02171.x.

Tite, M.S., 2008. Ceramic production, provenance and use. A review, Archaeometry 50 216–231. https://doi.org/10.1111/j.1475-4754.2008.00391.x.

Zhang, Z., Qiao, X., Yu, J., 2014. Microwave selective heating-enhanced reaction rates for mullite preparation from kaolinite, RSC Adv., 4, 2640,https://doi.org/10.1039/C3RA43767A.